

## Article

# Effect of Modifying Carbon Materials with Metal Phthalocynines and Palladium on Their Catalytic Activity in ORR

Andzhela Vladimirovna Bulanova <sup>1,\*</sup> , Roman Vladimirovich Shafigulin <sup>1</sup>, Kirill Yurievich Vinogradov <sup>1</sup> , Elena Olegovna Tokranova <sup>1</sup>, Evgenia Andreevna Martynenko <sup>2</sup> , Sergey Vladimirovich Vostrikov <sup>2</sup> and Vladimir Vladimirovich Podlipnov <sup>1</sup> 

<sup>1</sup> Institute of Natural Sciences, Samara University, 443086 Samara, Russia

<sup>2</sup> Chemistry Department, Samara State Technical University, 443100 Samara, Russia

\* Correspondence: av.bul@yandex.ru

**Abstract:** Bimetallic catalysts based on multi-walled carbon nanotubes (MWCNT), graphene oxide (GO) and ultradispersed diamonds (UDD) supports for the process of electroreduction of oxygen from alkaline electrolyte were obtained using high-temperature synthesis. The materials were characterized by low-temperature nitrogen adsorption, Raman spectroscopy, scanning electron microscopy and X-ray structure analysis. The synthesized bimetallic catalysts contain meso- and micropores. Based on the study by Raman spectroscopy, it is shown that high-temperature synthesis of MWCNT with metal phthalocyanines leads to doping of this material with nitrogen and the appearance of significant defects in the structure. Carbon nanotube-based catalysts showed enhanced activity compared to other carbon materials. Moreover, bimetallic catalysts based on cobalt phthalocyanine and palladium (MWCNT\_CoPc\_Pd) are characterized by higher activity on all carbon supports compared to materials contain on copper and palladium. The specific current density in the diffusion region of the MWCNT\_CoPc\_Pd catalyst is comparable to a commercial platinum electrode (Pt(20%)/C) and equals to 2.65 mA/cm<sup>2</sup>. The area of the electrochemically active surface of all the obtained catalysts was calculated from the CV data in a nitrogen atmosphere. The MWCNT\_CoPc\_Pd catalyst is characterized by high corrosivity: after 2500 revolutions, the current density in the diffusion region decreases by 7%, and, also, an increase in the values of  $E_{1/2}$  and  $E_{onset}$  is observed.

**Keywords:** electrochemical oxygen reduction; ORR; carbon nanotubes; graphene oxide; ultradispersed diamonds; doping of carbon materials; corrosion resistance; bimetallic electrocatalysts; metal phthalocyanines; palladium



**Citation:** Bulanova, A.V.; Shafigulin, R.V.; Vinogradov, K.Y.; Tokranova, E.O.; Martynenko, E.A.; Vostrikov, S.V.; Podlipnov, V.V. Effect of Modifying Carbon Materials with Metal Phthalocynines and Palladium on Their Catalytic Activity in ORR. *Catalysts* **2022**, *12*, 1013. <https://doi.org/10.3390/catal12091013>

Academic Editor: Yongjun Feng

Received: 29 July 2022

Accepted: 5 September 2022

Published: 7 September 2022

**Publisher's Note:** MDPI stays neutral with regard to jurisdictional claims in published maps and institutional affiliations.



**Copyright:** © 2022 by the authors. Licensee MDPI, Basel, Switzerland. This article is an open access article distributed under the terms and conditions of the Creative Commons Attribution (CC BY) license (<https://creativecommons.org/licenses/by/4.0/>).

## 1. Introduction

One of the promising alternative sources of electricity is fuel cells. Fuel cells are environmentally friendly, silent, fail-safe, and energy efficient. The work of fuel cells is based on the oxygen reduction reaction. This reaction is slow, and therefore, the use of catalysts is necessary. In modern industry, carbon-based platinum materials (~40% Pt) are used as a catalyst, which significantly increases the cost of fuel cells [1]. That is why the search for alternative catalysts for fuel cells is an urgent problem.

In recent years, the greatest interest has been directed to the development of catalysts on various carbon supports [2–5]. Examples of such materials are carbon black [6,7], carbon nanotubes [8,9], graphene oxide (for example, doped with nitrogen [10] or reduced graphene oxide [11]), as well as ultrafine diamonds [12].

Many works are devoted to the study of the influence of various modifiers: metals and alloys, monoatomic catalysts, or even metal-free catalysts are often used [13–15]. Moreover, silver, palladium, iron, nickel, and other metals and their alloys are used as modifying metals [16]. An example of monatomic catalysts can be materials with porphyrin-like

active centers of the  $\text{MeN}_4$  type (representing a metal atom surrounded by 4 nitrogen atoms) [17–19]. Metal-free catalysts are obtained by doping carbon materials with non-metals: nitrogen, sulfur, phosphorus, and other non-metals [20,21].

The catalyst can be modified with various metals. In its pure form, platinum, palladium, silver, and iridium, in decreasing order, show the highest activity [22]. Furthermore, it is possible to improve the properties of a catalyst by adding some amount of another metal to a metal with high catalytic activity. Thus, the addition of cobalt to platinum makes it possible to increase the diffusion current during ORR in an alkaline medium from 0.281 mA/ $\mu\text{g-Pt}$  to 0.460 mA/ $\mu\text{g-Pt}$  [23]. However, platinum alloys are expensive, so scientists are looking for an alternative by developing non-platinum catalysts for ORR. Catalysts based on palladium and cobalt oxide can serve as an example [24]. This catalyst raises the diffusion current of the ORR to the level of the diffusion current on the platinum catalyst. Moreover, this catalyst shows high stability: after 14,000 cycles,  $E_{\text{onset}}$  decreases by 12 mV versus 55 mV for platinum, while the  $E_{1/2}$  value remains the same, while it decreases by 41 mV on a platinum catalyst [24]. On the other hand, another effect is possible from the addition of a second metal. For a catalyst based on palladium and copper, an increase in its stability is observed in comparison with a palladium catalyst, and, also, self-activation of the catalyst occurs: during operation, part of the copper is washed out of the catalyst, which increases the effective area of palladium from 21.79 to 28.69  $\text{m}^2/\text{g}$  [25].

Another approach to modification is single-atom catalysts. Most often, porphyrins and phthalocyanines of various metals are used on various carriers: multi-walled carbon nanotubes, graphene, carbon based on titanium carbide, volcano carbon XC-72R, mesoporous carbon. For materials modified with iron and nickel phthalophanines, multiwalled carbon nanotubes and mesoporous carbon showed the highest activity [26]. Catalysts containing cobalt and nickel phthalocyanines ( $E_{1/2} = 0.83$  eV) [27], as well as iron and cobalt ( $E_{1/2} = 0.86$  eV) [28] performed well with similar supports. Moreover, high activity was achieved on MOFs modified with iron and cobalt ( $E_{1/2} = 0.864$  eV) [29] and on a covalent organic polymer modified with iron and nickel phthalocyanines ( $E_{1/2} = 0.803$  eV) [30].

The aim of this study was to investigate the activity of MWCNT, GO and UDD-based electrochemical oxygen reduction (ORR) catalysts doped with copper and cobalt phthalocyanines and modified with small amounts of palladium.

## 2. Results and Discussions

### 2.1. Synthesis of Catalysts

Accurate weights of carbon carriers (MWCNT, GO, and UDD), metal phthalocyanines, and palladium chloride were dissolved in 50 mL of ethyl alcohol and subjected to ultrasonic treatment for 4 h. The reaction mixture was dried in a muffle furnace at 90 °C and subjected to pyrolysis in a nitrogen atmosphere at 1000 °C with a heating gradient of 5 °C/min. The pyrolysis time was 1 h. The following catalysts were obtained: MWCNT\_CoPc\_Pd, MWCNT\_CuPc\_Pd, GO\_CoPc\_Pd, GO\_CuPc\_Pd, UDD\_CoPc\_Pd. The content of cobalt and copper was 10 wt.%, and palladium was 10 wt.%.

The synthesis of the MWCNT\_CoPc and MWCNT\_CuPc catalysts was carried out under similar conditions without using a palladium source at the initial stage of the synthesis.

The textural characteristics of the synthesized catalysts were studied by the method of low-temperature adsorption-desorption of nitrogen. The shape of the isotherms for the synthesized catalysts is displayed in Figure 1, and the textural parameters are shown in Table 1.

The total pore volume  $V_p$  (included both micropores and mesopores) was estimated by converting the amount of  $\text{N}_2$  gas adsorbed at a relative pressure of 0.99 to the liquid volume of the adsorbate ( $\text{N}_2$ ). The micropore volume  $V_{\text{micro}}$  was determined using the density functional theory (DFT).

The  $\text{N}_2$  adsorption-desorption isotherm for UDD are of type IV according to the IUPAC classification [31]. Furthermore, the isotherm exhibited a type  $\text{H}_2$  hysteresis loop at

medium-high pressures (from 0.45 to 0.95) produced by capillary condensation, which are typical for mesoporous materials.

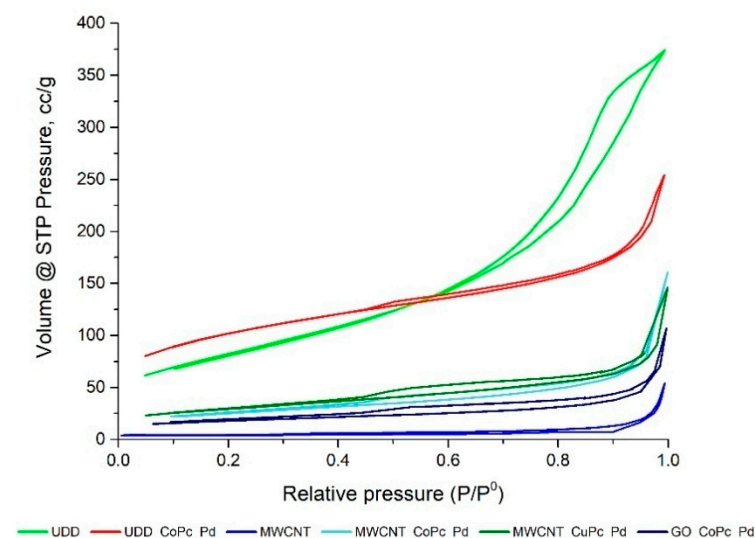


**Figure 1.** Low-temperature nitrogen adsorption-desorption isotherms for the synthesized catalysts.

**Table 1.** The textural characteristics of the supports and catalysts.

Sample	Surface Area, $S_{BET}$ , $m^2/g$	Pore Volume, $V_P$ , $cm^3/g$	Micropore Volume, $V_{micro}$ , $cm^3/g$
MWCNT	14.9	0.08	-
UDD	296.2	0.54	-
MWCNT_CoPc_Pd	52.1	0.23	0.02
MWCNT_CuPc_Pd	58.5	0.21	0.02
GO_CoPc_Pd	36.8	0.15	0.02
UDD_CoPc_Pd	88.8	0.25	0.11

All others adsorption-desorption isotherms are typical for a mesoporous material with a hysteresis loop at high partial pressures. The adsorption isotherm of GO is featureless, and did not show the pore structure (not shown in the figure), which is in agreement with that reported in the literature [32].

The pore size distribution obtained from the desorption branch of the isotherm shows the presence of mesopores with diameter 2–20 nm. No predominance of any particular pore size was observed.

According to BET analysis, a total specific surface area of 52–58  $m^2/g$  is obtained for the catalysts on MWCNT (MWCNT\_CoPc\_Pd and MWCNT\_CuPc\_Pd), which is larger than that of the pure MWCNT (14.9  $m^2/g$ ), which may be due to the decomposition of carbon oxygen compounds during the catalyst synthesis [33]. After the supporting of metals on the UDD, the surface area is decreased by about 3 times (see Table 1).

Figure 2 shows the Raman spectra and gives additional information about the surface of the synthesized carbon materials.

Two main peaks located at 1330 (D band) and 1590  $cm^{-1}$  (G band) are related to the disordered carbon and graphitic carbon peak, respectively. The process of doping the surface of carbon materials is usually accompanied by the formation of defects [34]. Table 2 shows the results of spectral analysis.

Doping of MWCNT with copper and cobalt phthalocyanines followed by modification with palladium leads to a significant decrease in the IG/ID ratio, as well as to a shift in the characteristic bands.

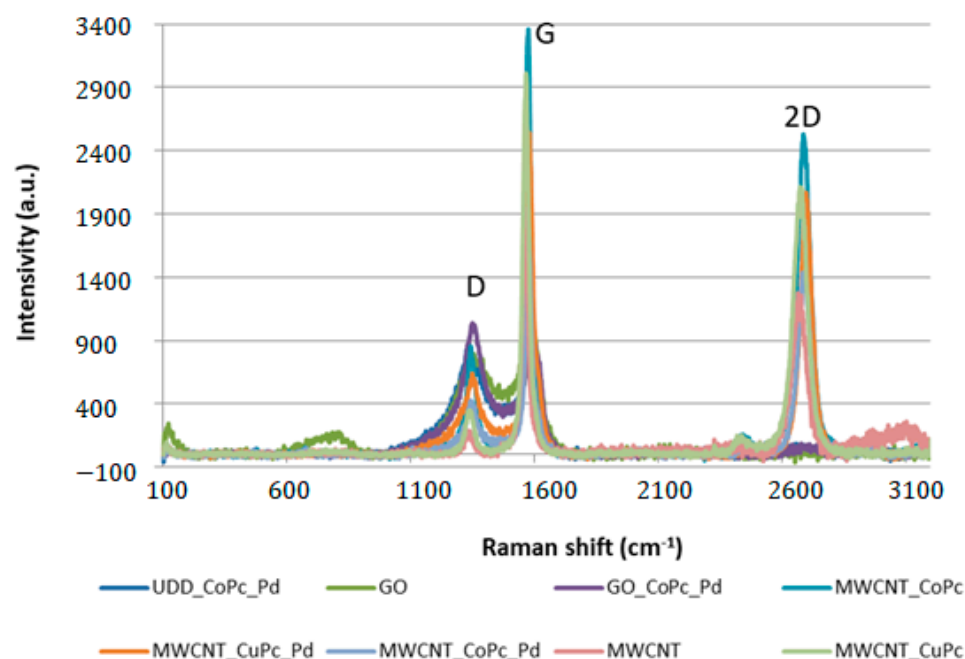


**Figure 2.** Raman spectra of the synthesized catalysts and the initial carbon supports.

**Table 2.** Results of the Raman spectra of the synthesized catalysts and initial carbon supports.

Sample	$\nu(\text{D}), \text{cm}^{-1}$	$\nu(\text{G}), \text{cm}^{-1}$	$\nu(2\text{D}), \text{cm}^{-1}$	ID	IG	I2D	IG/ID	I2D/IG
MWCNT	1336	1565	2666	187	1942	1273	10.4	0.66
MWCNT_CoPc_Pd	1345	1574	2684	425	1792	1436	4.2	0.80
MWCNT_CuPc_Pd	1350	1582	2698	639	2537	2068	4.0	0.82
GO	1357	1598	-	791	1004	-	1.3	-
GO_CoPc_Pd	1350	1588	-	1036	967	-	0.9	-
UDD_CoPc_Pd	1337	1593	-	852	845	-	1.0	-
UDD	1328	1608	-	3537	2898	-	0.8	-
MWCNT_CoPc	1343	1577	2690	855	3359	2504	3.9	0.75
MWCNT_CuPc	1338	1568	2674	348	3010	2114	8.6	0.70

In the process of high-temperature treatment of MWCNT with metal phthalocyanines, the intensity of the D peak also increases significantly. In parallel, there is a shift in the 2D peak and an increase in the I2D/IG ratio. All the above transformations of the Raman spectrum point to the doping with nitrogen process of MWCNT during its high-temperature treatment with metal phthalocyanines, as well as the formation of defects and disordering of the MWCNT structure [35,36]. It has been shown that high-temperature treatment of copper with phthalocyanine, without additional modification by palladium, does not lead to significant transformations of MWCNT. On the contrary, the treatment of cobalt with phthalocyanine is accompanied by serious changes in the MWCNT structure.

A similar modification of graphene oxide (GO) and ultra-dispersed diamonds (UDD) does not lead to additional formation of reaction centers, since these materials initially have a high degree of disorder and are characterized by a large number of defects on the surface. Some ordering of the UDD structure is observed after the synthesis and deposition of metals on its surface.

The morphology of the samples was studied by scanning electron microscopy (SEM). Photographs for the synthesized samples are shown in Figure 3.

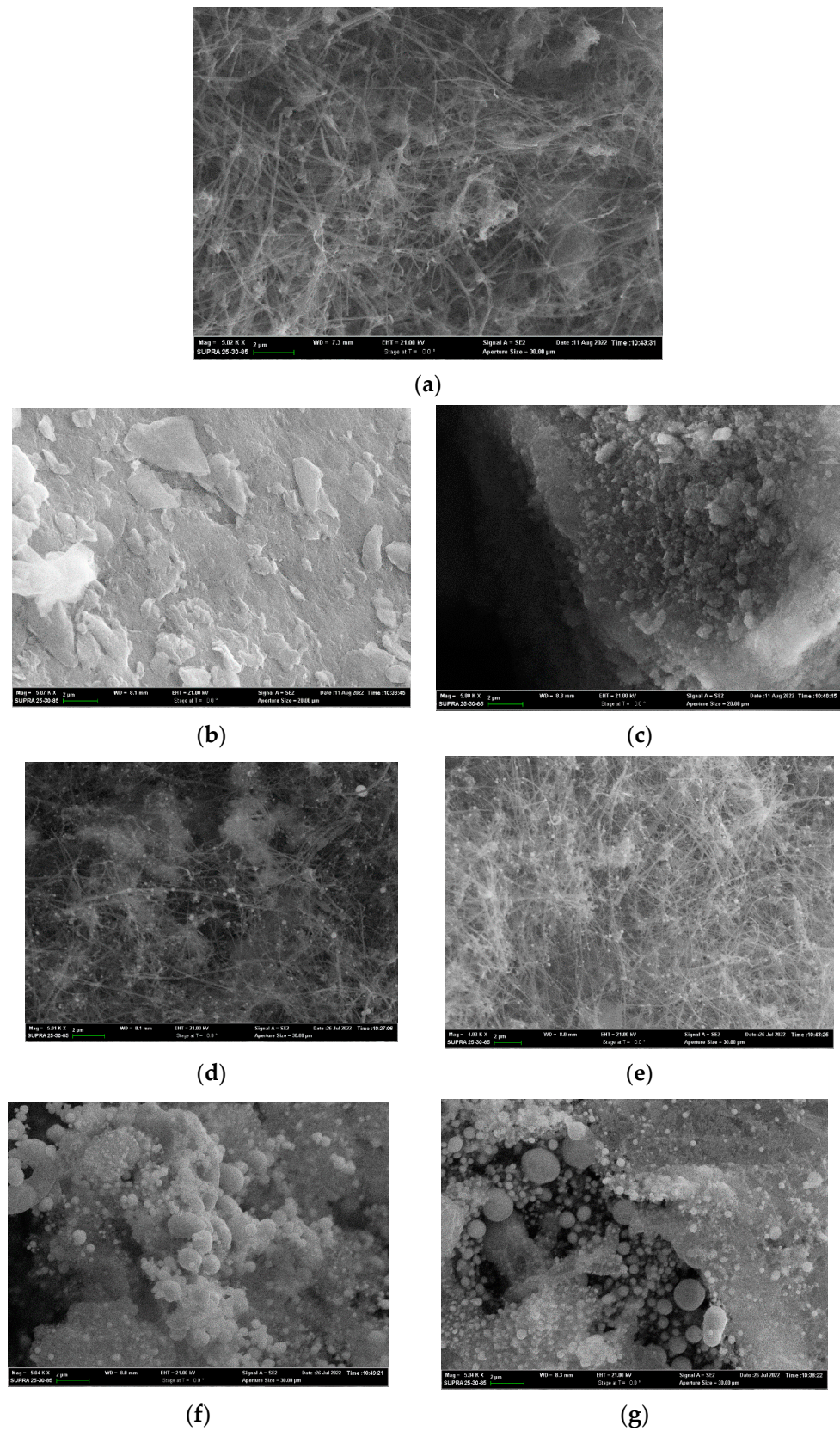


**Figure 3.** SEM photographs: (a) MWCNT (magnification 5000 times); (b) GO; (c) UDD; (d) MWCNT\_CoPc\_Pd (magnification 5000 times); (e) MWCNT\_CuPc\_Pd (magnification 4000 times); (f) UDD\_CoPc\_Pd (magnification 5000 times); (g) GO\_CoPc\_Pd (magnification 5000 times).

MWCNT-based catalysts have the structure of intertwining nanotubes on which metal particles are localized. It can be seen that the metal particles have a spherical structure and are regularly distributed in the bulk of the nanotubes; the average size of most particles does not exceed 100–150 nm. Catalysts based on UDD and GO have an amorphous structure in the form of irregularly shaped conglomerates. Metals on UDD and GO form sufficiently large particles and are unevenly distributed over the carrier surface.

For the qualitative identification and quantitative determination of metals, X-ray fluorescence analysis and thermogravimetric analysis were used, respectively. Figures 4 and 5 show the corresponding diagrams for some samples of the synthesized catalysts.

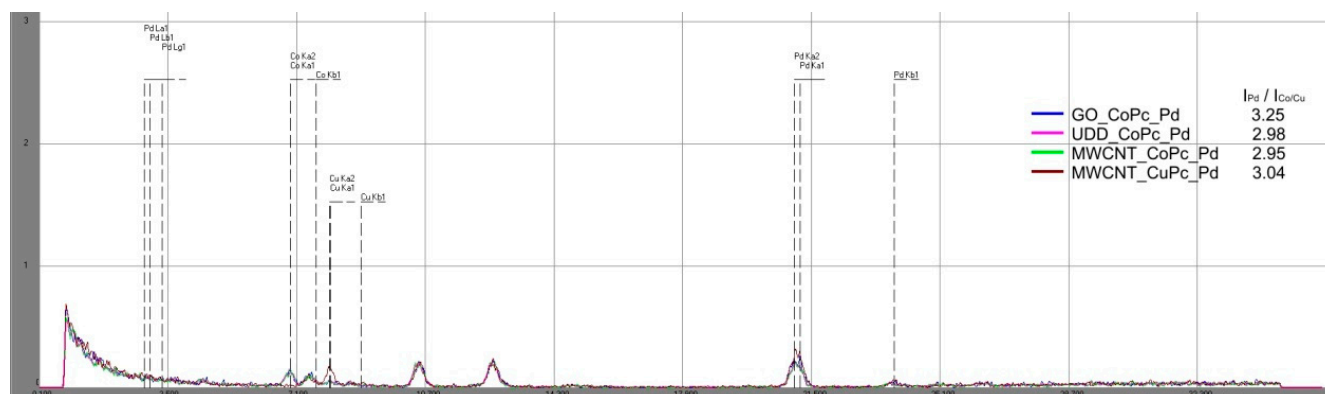


Figure 4. XRF spectrum of the studied samples.

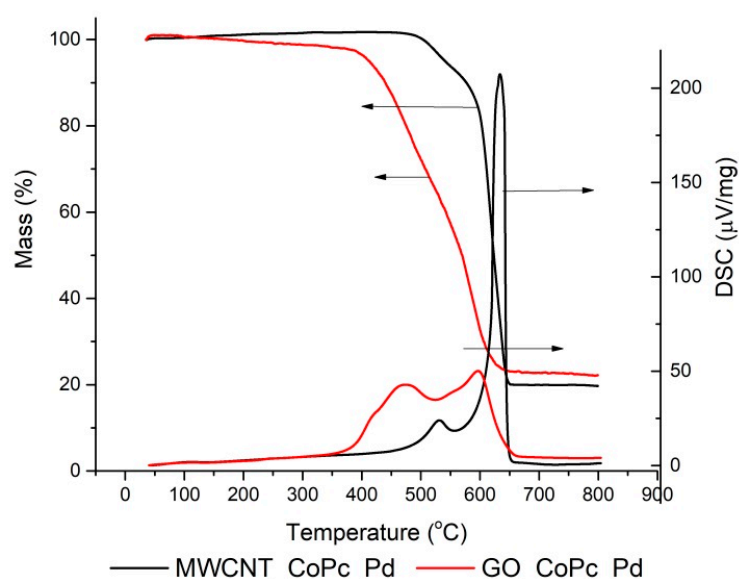
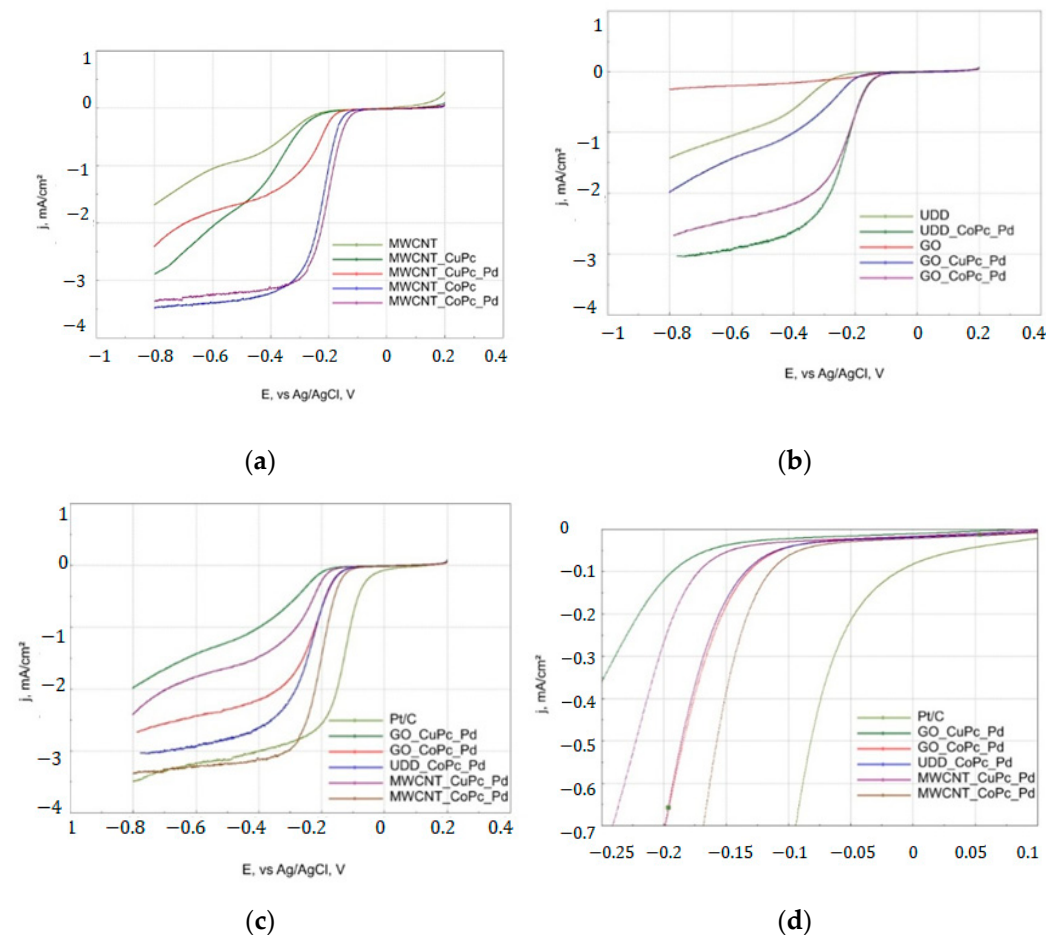


Figure 5. TGA—spectrum for some synthesized samples of catalysts.

X-ray fluorescence spectra contain only signals characteristic of copper, cobalt, and palladium metals in all samples under study. The values of the signal intensities ratios of palladium to cobalt and copper, the corresponding catalysts, are practically the same (about 3). This indirectly indicates the same atomic ratio of these metals in different samples of synthesized catalysts. Thermogravimetric analysis indicates a total metal content in the catalysts of about 20%. This is consistent with the calculated amounts in the process of synthesis of these catalysts. For other catalysts, the content was confirmed by the gravimetric method after combustion in oxygen.

## 2.2. Electrochemical Experiment

The electrochemical experiment was carried out in the modes of linear and cyclic voltammetry. Figure 6 shows linear voltammograms for the synthesized catalyst samples obtained using a rotating disk electrode.



**Figure 6.** Polarization curves for O<sub>2</sub> reduction on an electrode with various catalysts in an oxygen-saturated KOH solution with a concentration of 0.1 M: potential sweep rate 5 mV·s<sup>-1</sup>, electrode rotation speed 1500 rpm, catalyst loading about 80 μg·cm<sup>-2</sup>: (a) LV of catalysts based on MWCNT, (b) LV of catalysts based on GO and UDD, (c) LV of the studied catalysts, (d) kinetic part of LV of the studied catalysts.

Analyzing Figure 6a,b it can be seen that the non-metal modified carbon materials are generally characterized by low efficiency in the oxygen electroreduction reaction. Graphene oxide is the least active carbon matrix. Carbon nanotubes and ultra-dispersed diamonds are characterized by two pronounced waves of oxygen electroreduction process. Moreover, copper catalysts on all used substrates are also characterized by two pronounced waves on the polarization curves, and are significantly inferior in efficiency to cobalt-containing catalysts (Figure 6c,d). Two waves on the polarization curve can be related to the stepwise mechanism of electroreduction of oxygen from an alkaline electrolyte [37]. The first stage is characterized by a two-electron process of the formation of HO<sub>2</sub><sup>-</sup> ions, followed by the formation of water. Monometallic and bimetallic cobalt catalysts based on MWCNTs are characterized by a pronounced one plateau in the polarization curve and are characterized by a four-electron mechanism for the electroreduction of oxygen from an alkaline electrolyte [37]. In addition, some thermodynamic and kinetic characteristics of the reaction of oxygen electroreduction from an alkaline electrolyte were calculated based on the polarization curves (Table 3).

**Table 3.** Kinetic and thermodynamic parameters for ORR on the studied catalysts in KOH solution ( $O_2$ -saturated, 1500 rpm).

Catalyst	$j_{\text{dif}} (-0.75 \text{ V}),$ $\text{mA}/\text{cm}^2$	$E_{1/2}, \text{ V}$	$E_{\text{onset}}, \text{ V}$	$j_{\text{kin}} (-0.05 \text{ V}),$ $\text{mA}/\text{cm}^2$
Pt/C	3.41	−0.128	−0.053	0.2160
GO_CuPc_Pd	1.84	−0.321	−0.163	0.0168
GO_CoPc_Pd	2.64	−0.229	−0.116	0.0245
MWCNT_CoPc_Pd	3.33	−0.190	−0.109	0.0302
MWCNT_CuPc_Pd	2.20	−0.261	−0.139	0.0235
UDD_CoPc_Pd	3.04	−0.204	−0.127	0.0265
GO	− *	− *	− *	− *
MWCNT	1.52	−0.361	−0.247	0.0133
MWCNT_CuPc	2.76	−0.343	−0.165	0.0267
MWCNT_CoPc	3.45	−0.215	−0.116	0.0278
UDD	1.33	−0.370	−0.227	0.0049

\* The data are not shown due to the low activity of the catalyst and the low severity of the parameters.

Analyzing Table 3, it can be seen that the doping of carbon materials with metal phthalocyanines and palladium significantly increases the current density in both the diffusion and kinetic regions. The  $E_{1/2}$  and  $E_{\text{onset}}$  characteristics are also significantly shifted to a more positive area. The MWCNT\_CoPc monometallic catalyst is characterized by comparable current densities with the MWCNT\_CoPc\_Pd bimetallic catalyst but has more negative  $E_{1/2}$  and  $E_{\text{onset}}$  characteristics; the difference between these values on these catalysts is 0.025 and 0.007 V, respectively. The copper-containing MWCNT\_CuPc catalyst is characterized by much lower current densities compared to the cobalt-containing MWCNT\_CoPc catalyst; the difference in current densities  $j_{\text{dif}}$  for these catalysts is 0.69  $\text{mA}/\text{cm}^2$ . The  $E_{1/2}$  and  $E_{\text{onset}}$  values for MWCNT\_CuPc are much more negative than those for MWCNT\_CoPc. Additional modification of the copper-containing catalyst with palladium leads to a shift in the values of  $E_{1/2}$  and  $E_{\text{onset}}$  to a more positive region and, to an increase in the efficiency of the oxygen electroreduction process.

Comparative diagrams of the kinetic and thermodynamic characteristics of the process of oxygen electroreduction from an alkaline electrolyte were constructed for a more visual analysis of the characteristics of bimetallic catalysts on various carbon materials, (Figure 7).

Figure 7a shows a comparative diagram of current density values in the diffusion region at a potential of  $-0.75 \text{ V}$ . It has been established that cobalt-containing catalysts have higher diffusion current values compared to copper-containing catalysts. The MWCNT\_CoPc\_Pd catalyst is characterized by the highest current density in the diffusion region, and the GO\_CoPc\_Pd by the lowest. This is probably due to the fact that metal particles are more regularly distributed over the MWCNT surface, forming a large number of reaction centers for the oxygen electroreduction reaction. For graphene oxide, which is characterized by a large number of conglomerates and uneven distribution of metal particles on the surface, the number of reaction centers is lower. This may also be due to the larger specific surface area of the MWCNT\_CoPc\_Pd catalyst compared to GO\_CoPc\_Pd, which results in better adsorption of ORR participants on MWCNT\_CoPc\_Pd. Bimetallic cobalt catalyst based on UDD is characterized by an intermediate value of the current density in the diffusion region. The diffusion currents for the synthesized MWCNT\_CoPc\_Pd catalyst and the commercial platinum Pt/C catalyst are practically the same.

In the kinetic region (Figure 7b) at a potential of  $-0.05 \text{ V}$ , the platinum catalyst is characterized by a significantly higher current density compared to all synthesized catalysts. Figure 7c shows a comparative diagram of the values of the initial potential  $E_{\text{onset}}$  and the half-wave potential  $E_{1/2}$ . Cobalt catalysts are characterized by more positive values of these characteristics, compared with copper-containing catalysts on the corresponding carbon carriers. The MWCNT\_CoPc\_Pd catalyst has the closest  $E_{\text{onset}}$  and  $E_{1/2}$  values to the commercial platinum catalyst.

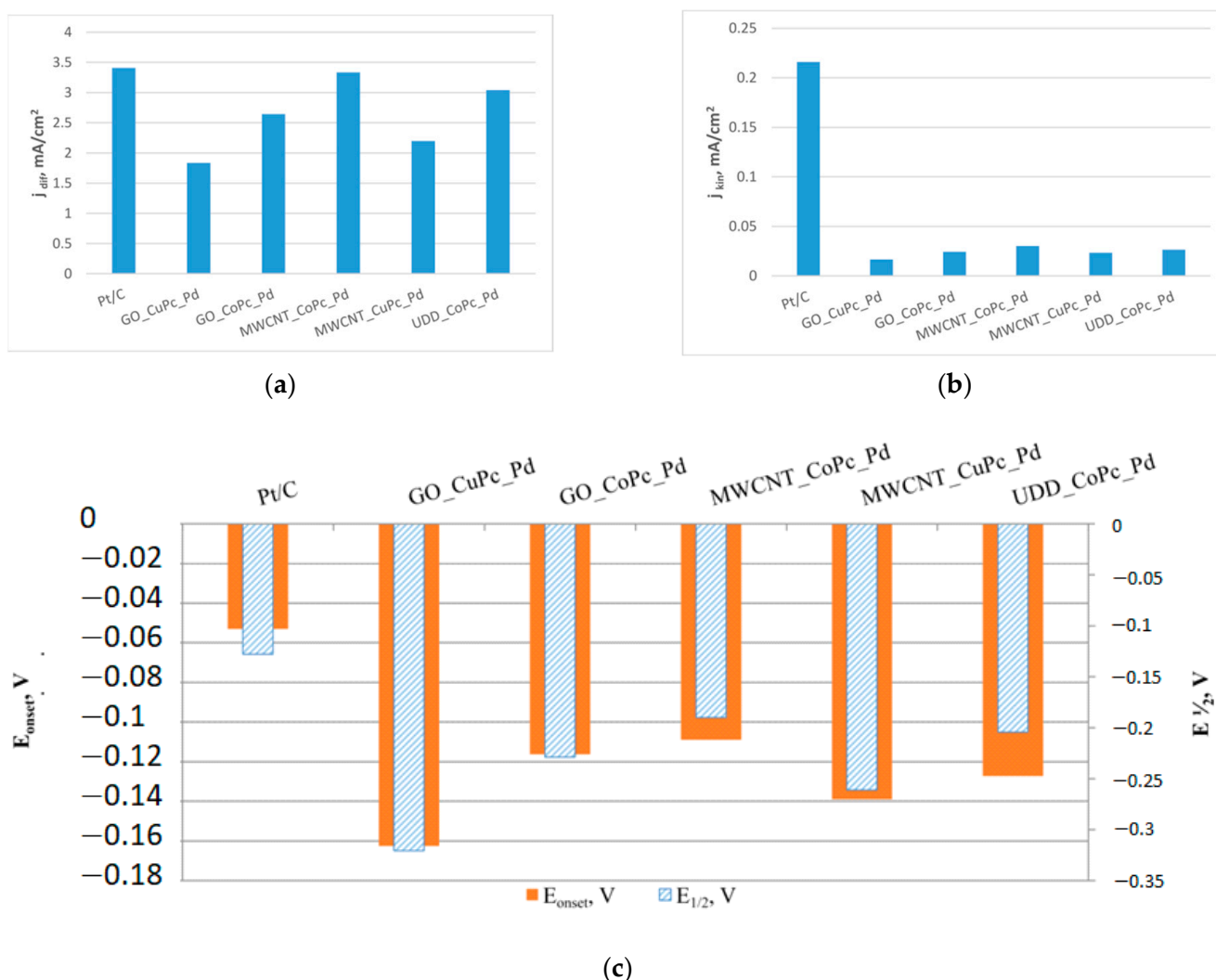


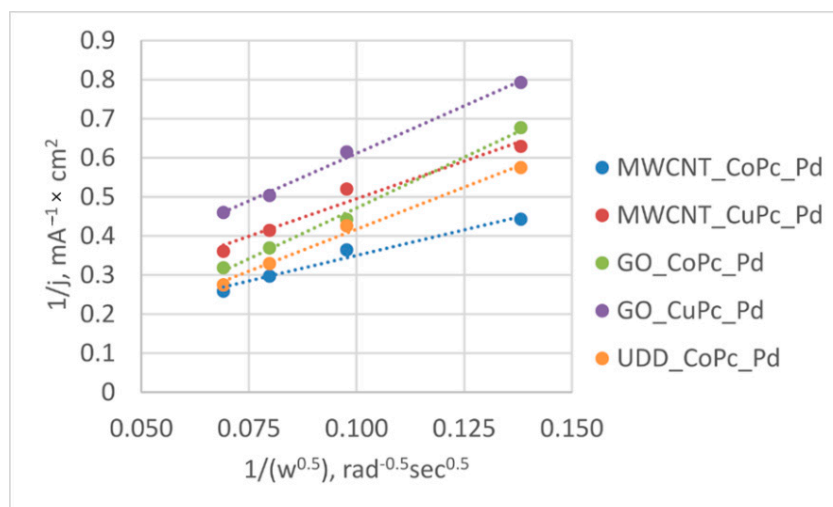
**Figure 7.** Comparative diagrams for the kinetic and thermodynamic characteristics of the electroreduction of oxygen from an alkaline electrolyte for the synthesized catalysts and a commercial platinum catalyst: (a) comparison chart by values  $j_{dif}$ ; (b) comparison chart by values  $j_{kin}$ ; (c) comparison chart by values  $E_{1/2}$  and  $E_{onset}$ .

To compare the activity of the catalysts, the Koutecky–Levich equation was used [38,39]:

$$\frac{1}{j} = \frac{1}{j_k} + \frac{1}{j_d} = \frac{1}{nFkC_{O_2}} + \frac{1}{0.62nFD_{O_2}^{2/3}\nu^{-1/6}C_{O_2}\omega^{1/2}}$$

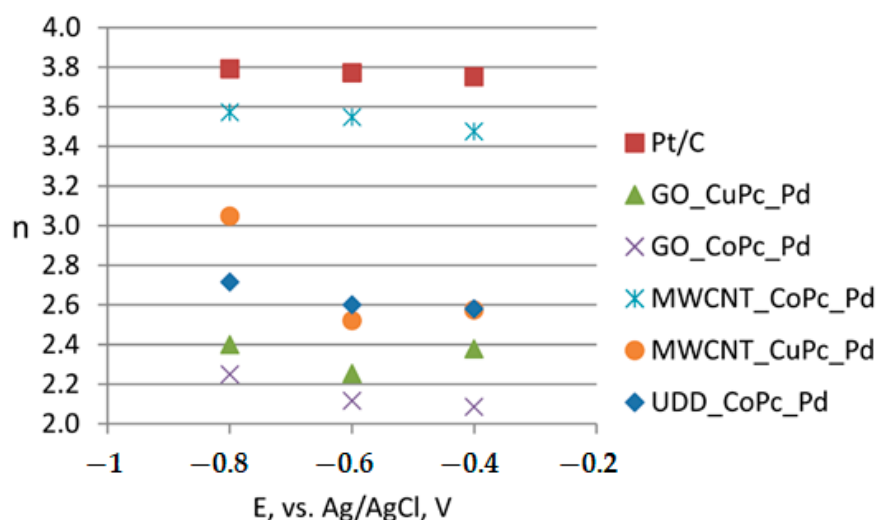
where  $j$  is the measured current density,  $j_k$  and  $j_d$  are the kinetic and diffusion-limited current densities, respectively,  $k$  is the electrochemical rate constant for  $O_2$  reduction,  $D_{O_2}$ —is the diffusion coefficient of oxygen ( $1.9 \times 10^{-5} \text{ cm}^2 \cdot \text{s}^{-1}$ ),  $C_{O_2}$ —is the concentration of oxygen in the bulk ( $1.2 \times 10^{-3} \text{ mol} \cdot \text{L}^{-1}$ ),  $\nu$  is the kinematic viscosity of the solution ( $0.01 \text{ cm}^2 \cdot \text{s}^{-1}$ ),  $\omega$  is the electrode rotation rate and  $n$  is the number of electrons transferred per  $O_2$  molecule.

Figure 8 shows the dependences in the coordinates of the Koutecky–Levich equation for all synthesized catalysts, obtained from the data on oxygen reduction at different speeds of rotation of the disk electrode in a 0.1 M KOH solution with  $O_2$ —saturated.



**Figure 8.** Dependences in the coordinates of the Koutecky–Levich equation at the potential  $-0.8$  V for all catalyst samples.

The dependences in the Koutetsky–Levich coordinates are linear with high determination coefficients (not less than 0.97). The number of electrons ( $n$ ) involved in the studied electrochemical reaction was calculated based on these dependences (Figure 9).



**Figure 9.** Calculated numbers of electrons transferred in the reaction as a function of the potential.

Extrapolation of the lines to a zero value of the reverse speed of rotation of the electrode leads to a value of the reverse current that is different from zero. This indicates that the process of electroreduction of oxygen on the synthesized catalysts from an alkaline electrolyte is under the control of a mixed diffusion-kinetic limiting stage [40]. The MWCNT\_CoPc\_Pd catalyst is characterized by the highest value of  $n$  equal to 3.6. For this catalyst, the number of electrons remains almost constant at all used potentials, and indirectly indicates the predominance of water in the final reaction product. For other synthesized catalysts, the value of  $n$  is much lower and sharply decreases when the potential is shifted to a more positive region. This indicates the predominance of the side reaction with the formation of the  $\text{HO}_2^-$  ion.

Figure 10 shows cyclic voltammograms in a nitrogen atmosphere for the synthesized bimetallic catalysts on various carbon substrates.

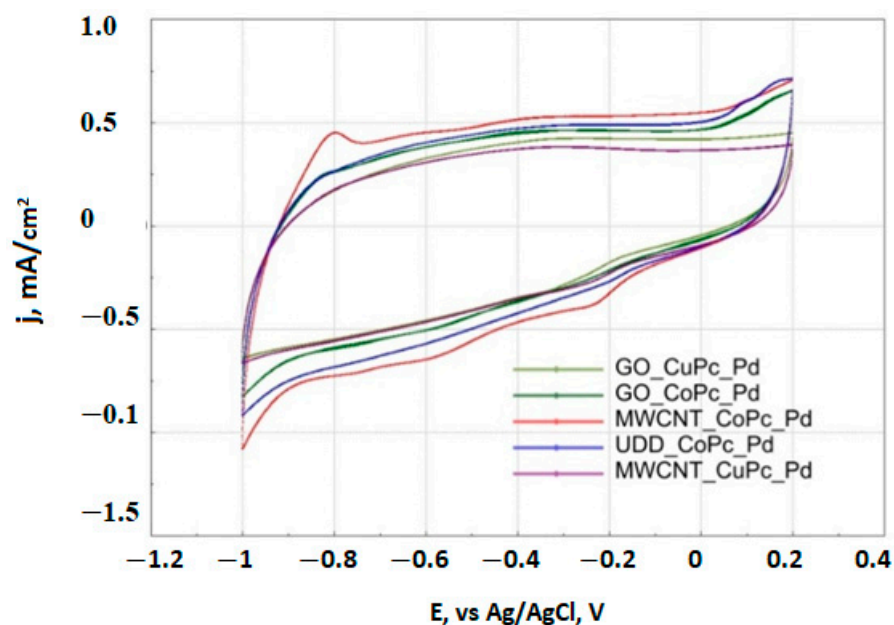


**Figure 10.** Cyclic voltammogram (CV) on electrode with various catalysts in de-aerated 0.1 M KOH solution: potential scan rate  $50 \text{ mV}\cdot\text{s}^{-1}$ .

Some cyclic voltammograms are characterized by two peaks in the cathode region around  $-0.230 \text{ V}$  and  $-0.600 \text{ V}$ . The peak with a potential of  $-0.230 \text{ V}$  probably characterizes the PdO reduction process and characterizes the availability of palladium in the process of oxygen electroreduction from an alkaline electrolyte [41]. The most active MWCNT\_CoPc\_Pd catalyst is characterized by a pronounced peak at  $-0.230 \text{ V}$ . The least efficient GO\_CuPc\_Pd and UDD\_CoPc\_Pd catalysts have almost no such peak. Apparently, the availability of palladium and its phase composition depend on the nature of the metal in the phthalocyanine structure and the carbon material. A signal at a potential of  $-0.6 \text{ V}$  is observed on cobalt catalysts with MWCNTs and GO. This signal is not traced on the UDD. It is difficult to identify this signal at this stage and requires further research.

Based on the CV, the amount of electricity in the cathode region ( $q_{\text{catod}}$ ) was calculated, which correlates with the specific electrochemical surface of the studied catalysts ( $S_{\text{EAS}}$ ) [42]. The dependence of the diffusion current on the amount of electricity (specific electrochemical surface) was plotted (Table 4 and Figure 11).

**Table 4.** Electrochemical active surface values ( $S_{\text{EAS}}$ ) for the catalysts ( $\theta = 50 \text{ mV/s}$ ).

Catalyst	$q(\text{as } S_{\text{EAS}}), \text{ mC/cm}^2$
Pt/C	26.4
GO_CuPc_Pd	8.6
GO_CoPc_Pd	9.7
MWCNT_CoPc_Pd	12.1
MWCNT_CuPc_Pd	9.6
UDD_CoPc_Pd	11.1

There is a tendency for the limiting current to increase with the increase in the electrochemically active surface.

The most active catalyst MWCNT\_CoPc\_Pd was tested for corrosion resistance by running 2500 cycles in a stream of oxygen. After cycling, a linear voltammogram was taken and the diffusion current was calculated at a potential  $-0.80 \text{ V}$ . (Figure 12).

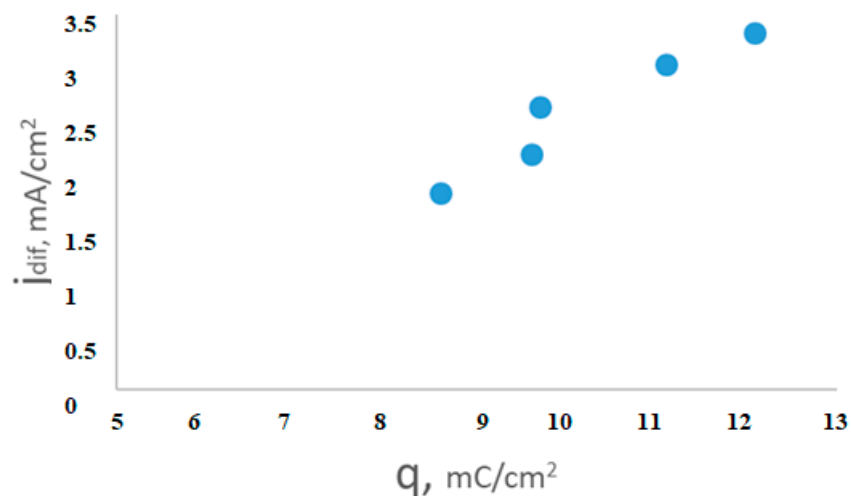
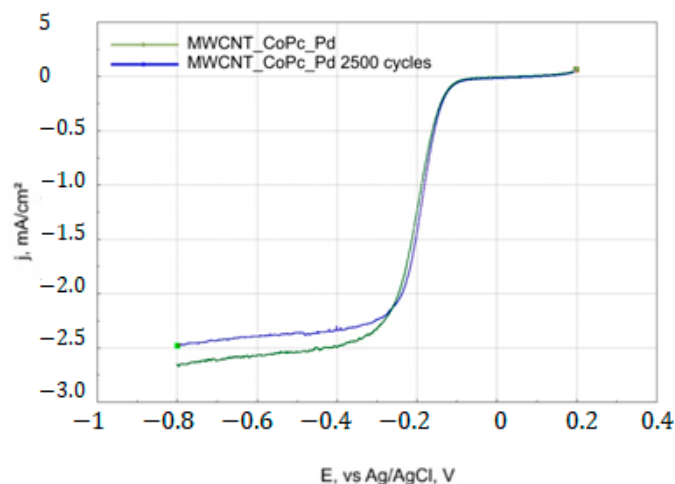
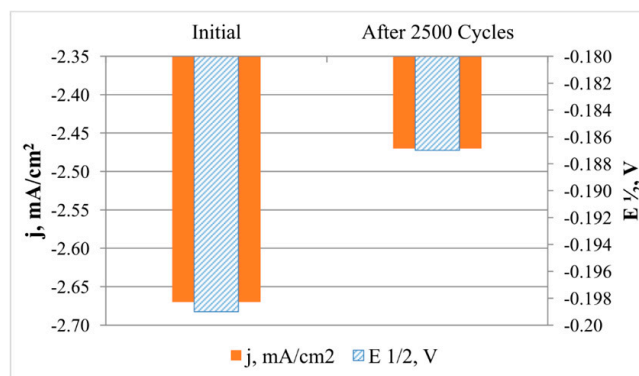


**Figure 11.** Influence of an electrochemically active surface on the limiting current for the synthesized catalysts.



(a)



(b)

**Figure 12.** Corrosion resistance test of the MWCNT\_CoPc\_Pd catalyst: (a) LV before and after 2500 cycles; (b) comparative diagram of diffusion current density ( $-0.80$  V) before and after 2500 cycles.

After 2500 cycles in an oxygen atmosphere, the current density in the diffusion region for the MWCNT\_CoPc\_Pd catalyst decreases by 7%, which indicates a high corrosion resistance of material in the studied process. It has also been found that the initial potential

and the half-wave potential are increased. A slight increase in the half-wave potential ( $\sim 0.01$  V) may be associated with the effect of catalyst self-activation [25], associated with the washing out of one of the catalyst components, leading to the exposure of the surface of the other component. A cobalt-palladium intermediate of such a phase composition can also be formed, which makes it possible to enhance the reaction of electroreduction of oxygen from an alkaline electrolyte

Table 5 compares the characteristics of the studied reaction obtained in this work with the literature data.

**Table 5.** Comparison of characteristics obtained in present work with literature data.

Catalyst	$E_{1/2}$ , V	$E_{onset}$ , V	Source
Pt/C	−0.128	−0.053	This work
GO_CoPc_Pd	−0.229	−0.116	This work
MWCNT_CoPc_Pd	−0.190	−0.109	This work
UDD_CoPc_Pd	−0.204	−0.127	This work
Pd@Au/RGO	−0.157	0.183	[43]
Pd@Ag/RGO	−0.174	0.183	[43]
nanoFeTSPc-0-MWCNT	−0.32	−0.020	[44]
nanoFeTSPc-s-MWCNT	−0.40	−0.200	[44]
FePc/SWCNT	−0.10	n/a	[45]

It can be seen that the synthesized bimetallic catalysts on MWCNT are characterized by  $E_{1/2}$  and  $E_{onset}$  characteristics comparable with some obtained in similar studies.

### 3. Materials and Methods

#### 3.1. Chemicals and Materials

The following materials were used in the work: “Aldrich” multi-walled carbon nanotubes (MWCNT) (>95% carbon, diameter 50–90 nm); Graphene oxide (GO) manufactured by “Rusgrafen” (carbon content—about 46 wt%, oxygen—about 49 wt%, hydrogen—about 2.5 wt%, sulfur—no more than 3 wt%, specific surface area—20 m<sup>2</sup>/G); ultradispersed diamonds (UDD) of “Singa”. Metal phthalocyanines and potassium hydroxide were purchased from “Aldrich”. Palladium chloride was purchased from abcr. For comparison, commercial (HiSPEC) catalyst 20 wt% Pt/C was used.

#### 3.2. Characteristics of Catalysts

The textural characteristics of the synthesized supports and catalysts were studied by low-temperature nitrogen adsorption using a Quantochrome Autosorb-1 porosimeter (Quantochrome instruments). The specific surface area was calculated using the Brunauer-Emmett-Teller (BET) model.

The qualitative analysis was carried out by the method of X-ray fluorescence (XRF) analysis on a BRA-18.

Thermogravimetric analyzes were performed on a STA 449 F3 Jupiter (NETZSCH) in the temperature range from 35 to 800 °C at a heating rate of 10 °C/min in an air flow with a flow rate of 200 mL/min.

The Raman analysis was performed under backscattering geometry on a Renishaw In Via micro-Raman spectrometer equipped with a Charged Coupled Device (CCD) detector, Ar-ion laser ( $\lambda = 532$  nm) and 1800 lines/mm grating with a spectral resolution of 1 cm<sup>−1</sup>. The excitation source was focused down to a 2  $\mu$ m spot with a laser power of about 1 to 5 mW.

The morphology of the synthesized samples was investigated by SEM using a scanning electron microscope CarlZeiss Supra 25.

#### 3.3. Electrochemical Experiment

The process of electrochemical reduction of oxygen from an alkaline electrolyte (0.1 N KOH solution) was studied by the potentiometric method on a CorrTest device in the

modes of linear and cyclic voltammetry (LV and CV). A three-electrode cell with a rotating disk electrode was used. A disk glassy carbon electrode with a working surface of  $0.071 \text{ cm}^2$  was used as a working electrode. A platinum electrode with a large surface was used as an auxiliary electrode; a silver chloride electrode was used as a reference electrode. Linear voltammetry was carried out in an oxygen-saturated KOH solution in the potential range of  $-800 \div 200 \text{ mV}$  and a potential sweep rate of  $5 \text{ mV/s}$ . LV was filmed at different speeds of rotation of the disk electrode:  $500 \div 2500 \text{ rpm}$ . CV was recorded in a nitrogen-deaerated KOH solution in the potential range of  $-1000 \div 200 \text{ mV}$ .

#### 3.4. Preparation of Catalytic Ink

Accurate weighing of catalysts ( $0.02 \text{ g}$ ) was dissolved in  $10 \text{ mL}$  of ethanol and  $200 \mu\text{L}$  of Nafion solution was added and ultrasonic treatment was performed for  $2 \text{ h}$ . Then, the catalytic ink was applied on the surface of the disk electrode (surface area  $0.071 \text{ cm}^2$ ) with a calculated load of  $80 \mu\text{g/cm}^2$  and dried on air for  $8 \text{ h}$  at a temperature of  $90 \text{ }^\circ\text{C}$ .

#### 4. Conclusions

Bimetallic catalysts based on copper and cobalt phthalocyanines with a small content of palladium on various carbon substrates—graphene oxide (GO), ultra-dispersed diamonds (UDD) and carbon nanotubes (MWCNT) have been synthesized. It is shown that the process of doping MWCNT with metal phthalocyanines leads to a significant change in the ordering of the surface of the carbon material with the formation of defects; no such effect is observed for UDD and GO. Analyzing the transformation of the Raman spectrum, it was found that high-temperature treatment of MWCNT with metal phthalocyanines leads to doping of the carbon material with nitrogen. Moreover, it was found using scanning electron microscopy that metal particles on MWCNT are distributed unregularly in the volume of nanotubes, which contributes to an increase in the number of reaction centers and, accordingly, an increase in the ORR efficiency. Bimetallic catalysts based on MWCNT are more efficient than the same catalysts based on GO and UDD. Catalysts based on GO, UDD, and MWCNT modified with cobalt show a higher catalytic activity in ORR compared to those modified with copper. Copper catalysts on all used carbon substrates are characterized by two pronounced waves on the polarization curves, which indicates a two-electron mechanism of the oxygen electroreduction reaction with the intermediate formation of the by-product  $\text{HO}_2^-$  ion. Bimetallic cobalt catalysts based on MWCNTs are characterized by a mechanism close to the four-electron mechanism of oxygen electroreduction from an alkaline electrolyte. The number of electrons participating in the studied reaction for MWCNT\_CoPc\_Pd is  $3.6$  at a potential of  $-0.8 \text{ V}$ . The current density in the diffusion region for the MWCNT\_CoPc\_Pd catalyst practically coincides with the commercial platinum Pt/C catalyst. Cyclic voltammograms in a nitrogen atmosphere for the most efficient cobalt catalysts based on MWCNT and GO are characterized by a peak at a potential of  $-0.230 \text{ V}$ , which indirectly indicates a great influence of the cobalt atom in the composition of the bimetallic intermediate on the oxygen electroreduction process. This signal is absent in the cyclic voltammogram of the least efficient GO\_CuPc\_Pd catalyst. Likewise, a linear correlation is observed between the current density in the diffusion region and the electrochemically active surface area of the catalyst ( $S_{\text{EAS}}$ ) for all synthesized catalysts. The closest in efficiency to a commercial platinum catalyst is the MWCNT\_CoPc\_Pd catalyst; it has a high corrosion stability—the decrease in current density after  $2500$  cycles in oxygen is about  $7\%$ . There is some increase in the initial potential and half-wave potential after corrosion testing. This is apparently due to the transformation of the bimetallic intermediate in the MWCNT\_CoPc\_Pd structure and the formation of the phase composition of the cobalt–palladium intermediate, which contributes to an increase in the activity of the catalyst.

**Author Contributions:** Conceptualization, A.V.B. and R.V.S.; methodology, K.Y.V. and V.V.P.; software, K.Y.V.; validation, A.V.B. and R.V.S.; formal analysis, E.O.T.; investigation, K.Y.V. and E.A.M.; re-sources, A.V.B.; data curation, R.V.S. and S.V.V.; writing—original draft preparation, K.Y.V.; writing—review and editing, A.V.B. and E.O.T.; visualization, K.Y.V.; supervision, A.V.B.; project administration, A.V.B.; funding acquisition, A.V.B. All authors have read and agreed to the published version of the manuscript.

**Funding:** This study was carried out with the financial support of the Russian Foundation for Basic Research project No. 19–53–80033. Studies of catalysts at the nanolevel carried out by scanning electron microscopy funded by Russian Federation Ministry of Science and Higher Education in the framework of the research performed by the laboratory “Photonics for a smart home and smart city” (State contract with the Samara University) (project FSSS-2021-0016).

**Data Availability Statement:** Data obtained during this study are included in the main text.

**Conflicts of Interest:** The authors declare no conflict of interest.

## References

1. Huya-Kouadio, J. Doe Hydrogen and Fuel Cells Program Record. 2017. Available online: [https://www.hydrogen.energy.gov/pdfs/17007\\_fuel\\_cell\\_system\\_cost\\_2017.pdf](https://www.hydrogen.energy.gov/pdfs/17007_fuel_cell_system_cost_2017.pdf) (accessed on 29 July 2022).
2. Han, A.; Zhang, Z.; Yang, J.; Wang, D.; Li, Y. Carbon-Supported Single-Atom Catalysts for Formic Acid Oxidation and Oxygen Reduction Reactions. *Small* **2021**, *17*, 2004500. [CrossRef]
3. Zhang, X.; Zhang, X.; Zhao, S.; Wang, Y.Q.; Lin, X.; Tian, Z.Q.; Shen, P.K.; Jiang, S.P. Precursor modulated active sites of nitrogen doped graphene-based carbon catalysts via one-step pyrolysis method for the enhanced oxygen reduction reaction. *Electrochim. Acta* **2021**, *370*, 137712. [CrossRef]
4. Mazzucato, M.; Daniel, G.; Mehmood, A.; Kosmala, T.; Granozzi, G.; Kucernak, A.; Durante, C. Effects of the induced micro- and meso-porosity on the single site density and turn over frequency of Fe-NC carbon electrodes for the oxygen reduction reaction. *Appl. Catal. B Environ.* **2021**, *291*, 120068. [CrossRef]
5. Wang, M.; Yang, W.; Li, X.; Xu, Y.; Zheng, L.; Su, C.; Liu, B. Atomically Dispersed Fe-Heteroatom (N, S) Bridge Sites Anchored on Carbon Nanosheets for Promoting Oxygen Reduction Reaction. *ACS Energy Lett.* **2021**, *6*, 379–386. [CrossRef]
6. Lopes, T.; Kucernak, A.; Malko, D.; Ticianelli, E.A. Mechanistic Insights into the Oxygen Reduction Reaction on Metal-N-C Electrocatalysts under Fuel Cell Conditions. *ChemElectroChem* **2016**, *3*, 1580–1590. [CrossRef]
7. Truong, V.M.; Yang, M.-K.; Yang, H. Functionalized Carbon Black Supported Silver (Ag/C) Catalysts in Cathode Electrode for Alkaline Anion Exchange Membrane Fuel Cells. *Int. J. Precis. Eng. Manuf. Technol.* **2019**, *6*, 711–721. [CrossRef]
8. Ruiz-Camacho, B.; Medina-Ramírez, A.; Fuentes-Ramírez, R.; Navarro, R.; Gómez, C.M.; Pérez-Larios, A. Pt and Pt–Ag nanoparticles supported on carbon nanotubes (CNT) for oxygen reduction reaction in alkaline medium. *Int. J. Hydrogen Energy* **2022**, *47*, 30147–30159. [CrossRef]
9. Liu, Y.; Zhao, B.; Zhang, Y.; Zhang, H.; Zhan, K.; Yang, J.; Li, J. Co-supported catalysts on nitrogen and sulfur co-doped vertically-aligned carbon nanotubes for oxygen reduction reaction. *RSC Adv.* **2016**, *6*, 32676–32684. [CrossRef]
10. Wu, G.; Nie, Y.; Zhang, D.; Zhang, C.; Guo, J.; Zhang, D.; Qi, G.; Jiao, W.; Yuan, Z. The MOF/GO-based derivatives with Co@CoO core-shell structure supported on the N-doped graphene as electrocatalyst for oxygen reduction reaction. *J. Chin. Chem. Soc.* **2020**, *67*, 1189–1194. [CrossRef]
11. Ning, R.; Tian, J.; Asiri, A.M.; Qusti, A.H.; Al-Youbi, A.O.; Sun, X. Spinel CuCo<sub>2</sub>O<sub>4</sub> Nanoparticles Supported on N-Doped Reduced Graphene Oxide: A Highly Active and Stable Hybrid Electrocatalyst for the Oxygen Reduction Reaction. *Langmuir* **2013**, *29*, 13146–13151. [CrossRef] [PubMed]
12. Van Hung, T.; Karunagaran, R.; Tung, T.T.; Dang, N.N.; Nguyen, S.X.; Losic, D. Nitrogen-doped carbon-coated nanodiamonds for electrocatalytic applications. *J. Phys. D Appl. Phys.* **2020**, *54*, 085303. [CrossRef]
13. Li, M.; Hu, Z.; Li, H.; Zhao, W.; Zhou, W.; Yang, Q.; Hu, S. Pt–Ni Alloy Nanoparticles via High-Temperature Shock as Efficient Electrocatalysts in the Oxygen Reduction Reaction. *ACS Appl. Nano Mater.* **2022**, *5*, 8243–8250. [CrossRef]
14. Xue, Z.; Zhang, X.; Qin, J.; Liu, R. TMN<sub>4</sub> complex embedded graphene as bifunctional electrocatalysts for high efficiency OER/ORR. *J. Energy Chem.* **2021**, *55*, 437–443. [CrossRef]
15. Wei, P.; Li, X.; He, Z.; Sun, X.; Liang, Q.; Wang, Z.; Fang, C.; Li, Q.; Yang, H.; Han, J.; et al. Porous N, B co-doped carbon nanotubes as efficient metal-free electrocatalysts for ORR and Zn-air batteries. *Chem. Eng. J.* **2021**, *422*, 130134. [CrossRef]
16. Sirirak, R.; Jarulertwathana, B.; Laokawee, V.; Susingrat, W.; Sarakonsri, T. FeNi alloy supported on nitrogen-doped graphene catalysts by polyol process for oxygen reduction reaction (ORR) in proton exchange membrane fuel cell (PEMFC) cathode. *Res. Chem. Intermed.* **2017**, *43*, 2905–2919. [CrossRef]
17. Nematollahi, P.; Barbiellini, B.; Bansil, A.; Lamoen, D.; Qingying, J.; Mukerjee, S.; Neyts, E.C. Identification of a Robust and Durable FeN<sub>4</sub>C<sub>x</sub> Catalyst for ORR in PEM Fuel Cells and the Role of the Fifth Ligand. *ACS Catal.* **2022**, *12*, 7541–7549. [CrossRef]
18. Yang, H.; Li, Z.; Kou, S.; Lu, G.; Liu, Z. A complex-sequestered strategy to fabricate Fe single-atom catalyst for efficient oxygen reduction in a broad pH-range. *Appl. Catal. B Environ.* **2020**, *278*, 119270. [CrossRef]

19. Ge, F.; Qiao, Q.; Chen, X.; Wu, Y. Probing the catalytic activity of M-N<sub>4</sub>-xO<sub>x</sub> embedded graphene for the oxygen reduction reaction by density functional theory. *Front. Chem. Sci. Eng.* **2021**, *15*, 1206–1216. [CrossRef]
20. Domínguez, C.; Pérez-Alonso, F.J.; Al-Thabaiti, S.A.; Basahel, S.N.; Obaid, A.Y.; Alyoubi, A.O.; de la Fuente, J.L.G.; Rojas, S. Effect of N and S co-doping of multiwalled carbon nanotubes for the oxygen reduction. *Electrochim. Acta* **2015**, *157*, 158–165. [CrossRef]
21. Mohammadi, F.; Tavakol, H. Synthesis of phosphorus doped carbon nanotubes using chemical vapor deposition. *Full-Nanotub. Carbon Nanostruct.* **2018**, *26*, 218–225. [CrossRef]
22. Wang, T.; Chutia, A.; Brett, D.J.L.; Shearing, P.R.; He, G.; Chai, G.; Parkin, I.P. Palladium alloys used as electrocatalysts for the oxygen reduction reaction. *Energy Environ. Sci.* **2021**, *14*, 2639–2669. [CrossRef]
23. Sravani, B.; Raghavendra, P.; Chandrasekhar, Y.; Reddy, Y.V.M.; Sivasubramanian, R.; Venkateswarlu, K.; Madhavi, G.; Sarma, L.S. Immobilization of platinum-cobalt and platinum-nickel bimetallic nanoparticles on pomegranate peel extract-treated reduced graphene oxide as electrocatalysts for oxygen reduction reaction. *Int. J. Hydrogen Energy* **2020**, *45*, 7680–7690. [CrossRef]
24. He, X.; Li, D.; Bai, Z.; Chang, F.; Qiao, J.; Yang, L. Multi-wall carbon nanotube-supported palladium-cobalt oxide nanoparticle as efficient catalyst for oxygen reduction reaction. *Ionics* **2019**, *25*, 5929–5937. [CrossRef]
25. Ma, M.; Zhu, W.; Shao, Q.; Shi, H.; Liao, F.; Shao, C.; Shao, M. Palladium-copper bimetallic nanoparticles loaded on carbon black for oxygen reduction and zinc-air batteries. *ACS Appl. Nano Mater.* **2021**, *4*, 1478–1484. [CrossRef]
26. Kumar, Y.; Kibena-Pöldsepp, E.; Mooste, M.; Kozlova, J.; Kikas, A.; Aruväli, J.; Käärik, M.; Kisand, V.; Leis, J.; Tamm, A.; et al. Iron and Nickel Phthalocyanine-Modified Nanocarbon Materials as Cathode Catalysts for Anion-Exchange Membrane Fuel Cells and Zinc-Air Batteries. 2022. Available online: <https://ssrn.com/abstract=4049705> (accessed on 29 July 2022).
27. Kumar, Y.; Kibena-Pöldsepp, E.; Kozlova, J.; Kikas, A.; Käärik, M.; Aruväli, J.; Kisand, V.; Leis, J.; Tamm, A.; Tammeveski, K. Bimetal Phthalocyanine-Modified Carbon Nanotube-Based Bifunctional Catalysts for Zinc-Air Batteries. *ChemElectroChem* **2021**, *8*, 2662–2670. [CrossRef]
28. Kumar, Y.; Kibena-Pöldsepp, E.; Kozlova, J.; Rahn, M.; Treshchalov, A.; Kikas, A.; Kisand, V.; Aruväli, J.; Tamm, A.; Douglin, J.C.; et al. Bifunctional Oxygen Electrocatalysis on Mixed Metal Phthalocyanine-Modified Carbon Nanotubes Prepared via Pyrolysis. *ACS Appl. Mater. Interfaces* **2021**, *13*, 41507–41516. [CrossRef]
29. Zhang, C.; Yang, H.; Zhong, D.; Xu, Y.; Wang, Y.; Yuan, Q.; Liang, Z.; Wang, B.; Zhang, W.; Zheng, H.; et al. A yolk-shell structured metal-organic framework with encapsulated iron-porphyrin and its derived bimetallic nitrogen-doped porous carbon for an efficient oxygen reduction reaction. *J. Mater. Chem. A* **2020**, *8*, 9536–9544. [CrossRef]
30. Liao, Z.; Wang, Y.; Wang, Q.; Cheng, Y.; Xiang, Z. Bimetal-phthalocyanine based covalent organic polymers for highly efficient oxygen electrode. *Appl. Catal. B Environ.* **2019**, *243*, 204–211. [CrossRef]
31. Sing, K.S. Reporting physisorption data for gas/solid systems with special reference to the determination of surface area and porosity (Recommendations 1984). *Pure Appl. Chem.* **1985**, *57*, 603–619. [CrossRef]
32. Zhao, Y.; Dong, F.; Han, W.; Zhao, H.; Tang, Z. Construction of Cu-Ce/graphene catalysts via a one-step hydrothermal method and their excellent CO catalytic oxidation performance. *RSC Adv.* **2018**, *8*, 1583–1592. [CrossRef]
33. Li, F.; Cao, B.; Zhu, W.; Song, H.; Wang, K.; Li, C. Hydrogenation of Phenol over Pt/CNTs: The Effects of Pt Loading and Reaction Solvents. *Catalysts* **2017**, *7*, 145. [CrossRef]
34. Jeon, I.Y.; Noh, H.J.; Baek, J.B. Nitrogen-Doped Carbon Nanomaterials: Synthesis, Characteristics and Applications. *Chem. Asian J.* **2020**, *15*, 2282–2293. [CrossRef] [PubMed]
35. Das, A.; Pisana, S.; Chakraborty, B.; Piscanec, S.; Saha, S.K.; Waghmare, U.V.; Novoselov, K.S.; Krishnamurthy, H.R.; Geim, A.K.; Ferrari, A.C.; et al. Monitoring dopants by Raman scattering in an electrochemically top-gated graphene transistor. *Nat. Nanotechnol.* **2008**, *3*, 210–215. [CrossRef]
36. Lin, Y.C.; Lin, C.Y.; Chiu, P.W. Controllable graphene N-doping with ammonia plasma. *Appl. Phys. Lett.* **2010**, *96*, 133110. [CrossRef]
37. Wu, J.; Zhang, D.; Wang, Y.; Hou, B. Electrocatalytic activity of nitrogen-doped graphene synthesized via a one-pot hydrothermal process towards oxygen reduction reaction. *J. Power Source* **2013**, *227*, 185–190. [CrossRef]
38. Levich, V.G. *Physicochemical Hydrodynamics*; Prentice-Hall: Englewood Cliffs, NJ, USA, 1962; pp. 689–700. Available online: <https://onlinelibrary.wiley.com/doi/book/10.1002/0471725137> (accessed on 29 July 2022).
39. Koutecky, J.; Levich, V.G. The use of a rotating disk electrode in the studies of electrochemical kinetics and electrolytic processes. *Russ. J. Phys. Chem. A* **1958**, *32*, 1565–1575.
40. Kruusenberg, I.; Matisen, L.; Shah, Q.; Kannan, A.M.; Tammeveski, K. Non-platinum cathode catalysts for alkaline membrane fuel cells. *Int. J. Hydrogen Energy* **2012**, *37*, 4406–4412. [CrossRef]
41. Jiang, L.; Hsu, A.; Chu, D.; Chen, R. A highly active Pd coated Ag electrocatalyst for oxygen reduction reactions in alkaline media. *Electrochim. Acta* **2010**, *55*, 4506–4511. [CrossRef]
42. Bogdanovskaya, V.; Vernigor, I.; Radina, M.; Andreev, V.; Korchagin, O.; Novikov, V. Carbon Nanotube Modified by (O, N, P) Atoms as Effective Catalysts for Electroreduction of Oxygen in Alkaline Media. *Catalysts* **2020**, *10*, 892. [CrossRef]
43. Raghavendra, P.; Reddy, G.V.; Sivasubramanian, R.; Chandana, P.S.; Sarma, L.S. Reduced graphene oxide-supported Pd@Au bimetallic nano electrocatalyst for enhanced oxygen reduction reaction in alkaline media. *Int. J. Hydrogen Energy* **2018**, *43*, 4125–4135. [CrossRef]

44. Fashedemi, O.O.; Ozoemena, K.I. Oxygen reduction reaction at MWCNT-modified nanoscale iron (II) tetrasulfophthalocyanine: Remarkable performance over platinum and tolerance toward methanol in alkaline medium. *RSC Adv.* **2015**, *5*, 22869–22878. [[CrossRef](#)]
45. Dong, G.; Huang, M.; Guan, L. Iron phthalocyanine coated on single-walled carbon nanotubes composite for the oxygen reduction reaction in alkaline media. *Phys. Chem. Chem. Phys.* **2012**, *14*, 2557–2559. [[CrossRef](#)] [[PubMed](#)]